Research Article | Vol. 29, No. 2 / 18 January 2021 / Optics Express 865
Optics EXPRESS

Enhanced optical pulse broadening in free-space optical links due to the radiative effects of atmospheric aerosols

K. SUNILKUMAR,[1,2,*] N. ANAND,[1,3] S. K. SATHEESH,[1,3] K. KRISHNA MOORTHY,[1] AND G. ILAVAZHAGAN[2]

[1] *Centre for Atmospheric and Oceanic Sciences, Indian Institute of Science, Bengaluru 560012, India*
[2] *Centre for Photonics and LIDAR Research, Hindustan Institute of Technology and Science, Chennai 603103, India*
[3] *DST-Centre of Excellence in Climate Change, Divecha Centre for Climate Change, Indian Institute of Science, Bengaluru 560012, India*
[*] *sunilkumark@iisc.ac.in*

Abstract: Propagation through turbulent media produces complex amplitude fluctuations and temporal spreading of narrow optical pulses. Light-absorbing aerosols present in the atmospheric transmission path will perturb the refractive index structure parameter (C_n^2) through atmospheric heating. The consequent enhancement in broadening and attenuation of ultrashort (femtosecond) optical pulses has been calculated by combining multi-satellite observations, radiosonde profiles and computational radiative transfer. It is shown that narrower optical pulses are more vulnerable to aerosol-induced impairments while broader pulses are more resilient, notwithstanding three to four orders of enhanced optical scintillation.

1. Introduction

Data carrying potential of optical communication links has increased significantly in the past two decades. This has set off new research initiatives in both optical signal design and channel modelling, pushing forward the conventional frontiers of wireless communication systems [1,2]. Further, cellular towers and terrestrial backhaul networks operating in traditional radio frequency (RF) technology are drained of bandwidth resource to meet large volume data transfer requirements. Free-Space Optical (FSO) communication systems are potential auxiliary for such data straining backhaul networks [2]. FSO communication systems exploit different beam shapes and ultrashort pulses due to their potential ability to resist detrimental influence of atmospheric channel effects such as convective turbulence and atmospheric extinction. Despite possessing the potential to replace existing RF systems, FSO links are susceptible to atmospheric turbulence effects such as optical scintillation, pulse broadening, beam wandering etc. and signal loss resulting from the light absorption and scattering produced by atmospheric aerosols [1–3].

Aerosols are tiny, suspended particles in the atmosphere which are known to influence the radiation budget of the Earth-atmosphere system through scattering and absorption of solar radiation [4]. Their concentration and size change both temporally and spatially and mix dynamically with different species of its own leading to a heterogeneous anisotropic distribution [5]. The chemical and optical properties of atmospheric aerosols determine their absorption and scattering characteristics. Atmospheric aerosol forward scattering effects are significantly higher along with dominant atmospheric turbulence effects [6,7]. Aerosol black carbon (BC, also called as soot), originating from the incomplete combustion of carbonaceous fuels and injected into the atmosphere, significantly contribute to the absorption of solar radiation owing to its broad-band absorption in the visible and near-infrared spectra [8]. These highly absorbing aerosols are known to produce substantial heating of the lower atmosphere, where they are abundant [8,9]. A recent

#409794 https://doi.org/10.1364/OE.409794
Journal © 2021 Received 10 Sep 2020; revised 1 Nov 2020; accepted 2 Nov 2020; published 5 Jan 2021

Optics EXPRESS

study has shown that the signal extinction due to BC absorption may be compensated by the large reduction in the refractive index structure parameter, C_n^2, due to BC-induced atmospheric warming which can bring down the FSO link outage probability [10]. It has been shown recently that both scattering, and absorption of aerosols have influence on target identification systems and image restoration process [11]. Analytical formulations for pulsed beam wave propagation through turbulence [12] and pulse broadening [13] have been made in the past using two-frequency mutual coherence function. Analytical expression for two-frequency mutual coherence function and pulse shape on propagation through a random media were reported [14]. Effects of turbulent media on FSO systems have also been investigated [15–17]. It is also reported that increased loading of BC aerosols in the atmospheric channel results in significant signal deterioration during stable atmospheric conditions [18] by significantly degrading the bit error rate (BER) performance of FSO communication links [19] and the horizontal propagation of optical signals experience varied extinction due to the presence of humid aerosols [20]. Detrimental effects of particulates in the atmosphere manifest itself through further degradation in the received power and influence the signal to noise ratio (SNR) and BER performance [21]. It is interesting to note that the aerosol induced regional warming affects outage probability and it influences the pulse propagation characteristics by modulating the optical turbulence [22]. Recently, it was reported that the local warming produced by absorbing aerosols can alter the refractive index of an atmospheric channel [23]. However, the impact of the radiative effects of atmospheric aerosols (through the aerosol-induced atmospheric warming) on broadening of ultrashort optical pulses has not been investigated earlier. Under this backdrop, we study the problem of propagation of ultrashort optical pulses through turbulent atmosphere and its additional broadening and energy redistribution due to the radiative effects of aerosol particles through thermodynamic observations and radiative transfer theory.

2. Optical pulse broadening: analytical approach

Fourier spectra of optical pulses contain large number of frequency components and it increases as the pulse become narrower. A dispersive medium such as atmosphere offers deleterious effects on such ultrashort pulses, resulting in broadening of the pulses, since different spectral components undergo disparate velocity retardation. The spectral dependence of velocity originates from the frequency dependence of propagation constant (β) of optical pulse. Taylor series expansion of 'β' around the angular frequency of the carrier (ω_0), is given as [24,25]

$$\beta(\omega) = \beta_0 + \beta_1(\Delta\omega) + \frac{\beta_2}{2}(\Delta\omega)^2 + \frac{\beta_3}{6}(\Delta\omega)^3 + \dots \tag{1}$$

where $\Delta\omega=\omega-\omega_0$ is the spectral width of the pulse and the last two terms indicate the second order dispersion (group velocity dispersion – GVD) and third order dispersion (TOD) respectively. Parameters 'β_2' and 'β_3' can be obtained by inserting n=2 and 3 respectively in

$$\beta_n(\omega) = \left(\frac{d^n\beta}{d\omega^n}\right)_{\omega=\omega_0} \tag{2}$$

Propagation characteristics and pulse broadening depend on the second order dispersion for optical pulses in the nanosecond to picosecond regime, whereas the third order dispersion becomes dominant for femtosecond pulses. The refractive index is the most important parameter governing the light propagation through a medium, and for a gaseous atmosphere, it is a function of space as well as time. Considering the frequency dependence of the refractive index, the propagation constant can be expressed as [25]

$$\beta(\omega) = \frac{\omega}{c}\left[1 + 77.6\left(1 + 7.52\times10^{-15}\left(\frac{\omega}{2\pi\nu}\right)^2\right)\frac{P(h)}{T(h)}\times10^{-6}\right] \tag{3}$$

Optics EXPRESS

where 'ν' is the speed of spectral components in meters per second. The different spectral components undergo different velocity retardation due to the dispersive nature of the medium (frequency dependence of the refractive index of the air). Parameter 'h' is the altitude in meters, 'P(h)' and 'T(h)' indicate altitude dependent pressure in millibars and temperature in Kelvin, respectively.

3. Materials and methodology

Interaction of solar radiation with atmospheric aerosols are generally studied through radiative transfer (RT) theory. The general form of RT equation for the plane-parallel atmosphere is given by [26]

$$\cos\theta \frac{dI(z;\theta,\phi)}{k\rho dz} = -I(z;\theta,\phi) + J(z;\theta,\phi) \tag{4}$$

where 'θ' and 'ϕ' are elevation and azimuth angles, 'k' is the mass extinction cross-section, 'ρ' is the density of the medium, and 'J' is the Planck function used to represent the source function. The vital parameter which governs the optical signal propagation in FSO communication links is the refractive index structure parameter (C_n^2), which is modulated by the atmospheric aerosol induced warming through the net atmospheric forcing (ΔF). More details may be found in Ref. [23]. To solve the RT equation, we have employed a model based on the discrete ordinate method [27]. Meteorological data collected through radiosonde are amongst the most used and precise techniques to derive the vertical profile of atmospheric thermodynamics [28]. Radiosonde measured atmospheric thermodynamics data during March, April, and May (MAM) of 2012 over Chennai (13.08° N, 80.27° E, 6.7 m amsl), a metropolitan city located on the south-eastern coast of India, acquired from the University of Wyoming repository are used in this study. The constancy of absorbing BC aerosols is observed during earlier measurements in this selected location [29]. High-resolution balloon measurements and multi-satellite observations coupled with an RT model have shown the strong influence of absorbing aerosols on the vertical distribution of C_n^2 [30]. We have used level 2 aerosol extinction coefficient profiles derived from Cloud Aerosol Lidar with Orthogonal Polarization (CALIOP) onboard Cloud-Aerosol Lidar, and Infrared Pathfinder Satellite Observations (CALIPSO) and these values were normalized using Moderate Resolution Imaging Spectroradiometer (MODIS) onboard Terra satellite-derived aerosol optical depth (AOD). The surface reflectance data centered at seven wavelength bands in the range 0.469 - 2.13 μm were obtained from MODIS. These data were input to the Santa Barbara DISORT Atmospheric Radiative Transfer (SBDART) model [31], which is centered on a group of well tested and consistent physical models developed by the atmospheric science community over the past decades. Optical Properties of Aerosols and Clouds (OPAC), a Mie scattering model [32], was employed for deriving the aerosol scattering properties, while radiosonde profiles were used for atmospheric thermodynamic parameters. Considering the large residence time of atmospheric aerosols [33], we have derived atmospheric heating rate, and aerosol perturbed refractive index structure parameter (C_n^2*) for one day, from aerosol radiative forcing calculations, performed using SBDART at zero zenith angle following [10,23]. The refractive index structure parameter is

$$C_n^2 = a^2 L_0^{\frac{4}{3}} M^2 \tag{5}$$

$$M = -79 \times 10^{-6} \left(\frac{P}{T^2}\right) \left(\frac{dT}{dz} + \gamma\right) \tag{6}$$

where 'L_0' is the outer scale of turbulence, 'γ' is the dry adiabatic lapse rate (9.8 K/km), dT/dz is the vertical temperature gradient and a^2 is usually taken as 2.8 [28]. We define the broadening factor under normal atmospheric conditions (BF_{normal}) as the ratio of the pulse width (Ω_1) at

Optics EXPRESS

the receiver under aerosol-unperturbed conditions to the initial pulse width (Ω_0). This can be estimated from [24] as

$$\left(\frac{\sigma_1}{\sigma_0}\right)^2 = \left(1 + \frac{C\beta_2 z}{2\sigma_0^2}\right)^2 + \left(\frac{\beta_2 z}{2\sigma_0^2}\right)^2 + (1 + C^2)^2\left(\frac{\beta_3 z}{4\sqrt{2}\sigma_0^3}\right)^2 \tag{7}$$

where 'z' is the propagation length, $\sigma_0 = \Omega_0/\sqrt{2}$ is the root mean square (RMS) width of the input Gaussian pulse, 'σ_1' is the RMS width of the received pulse and 'C' represents the chirp parameter. A typical value of C = 2 has been chosen in this analysis. The estimated values at altitude 1.75 km for 'β_2' and 'β_3' are 1.18×10^{-35} s^2 m^{-1} and 9.37×10^{-45} s^3 m^{-1}, respectively. These values have been chosen to plot Fig. 1. We have utilized observed thermodynamic profiles from GPS radiosonde to estimate BF_{normal}. Pulse broadening produced due to atmospheric dispersion without considering the turbulence and aerosol effects can be found in [34]. The enhanced optical turbulence affects pulse propagation parameters, which can be characterized through the optical signal intensity distribution at the receiver. In the presence of optical turbulence, the on-axis mean intensity is given by [35]:

$$I(r, t, z) = \frac{\Omega_0}{\Omega_2} \exp\left(\frac{-2r^2}{{W_0}^2}\right) \exp\left[-\frac{2(t - z/c)^2}{\Omega_2^2}\right] \tag{8}$$

where 'r' is the vector in the transverse plane at a propagation distance 'z' from the source with an initial pulse width of 'Ω_0', 'W_0' is the spatial radius of the transmitted beam, and 'Ω_2' is an estimate of the received pulse half-width under aerosol perturbed conditions given by

$$\Omega_2 = (\Omega_0^2 + 8\psi)^{1/2} \tag{9}$$

where the 'ψ' is defined by

$$\psi = \frac{0.3908\ C_n^2\ z\ L_0^{5/3}}{c^2} \tag{10}$$

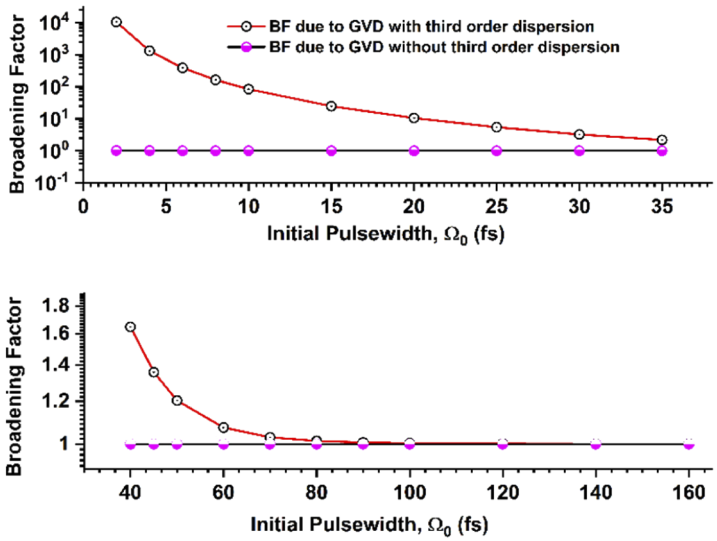

Fig. 1. Variation of Broadening Factor (BF_{normal}) due to the Group Velocity Dispersion (GVD) and Third Order Dispersion (TOD) with initial pulse width. The large impact of TOD on pulses with pulse width below 40 fs may be observed from the top panel.

Optics EXPRESS

where $L_0 = 10$ m, is the outer scale of turbulence, was estimated through the radiosonde measured thermodynamic profiles, and c is the velocity of light in vacuum.

4. Results and discussion

We have divided this section into two, first for framing the unperturbed conditions (where the perturbations due to aerosols are not considered), which sets the lower limit of initial pulse width (Ω_0) and for the second part discussing the enhanced pulse broadening due to aerosol radiative heating. Results from the first section establish the rationale for the selection of initial pulse width (Ω_0) for the remaining analysis.

4.1. Unperturbed atmospheric channel conditions (no aerosol perturbation)

By invoking Eq. (7), we show, in Fig. 1, the variation of the broadening factor BF_{normal} against initial pulse width (Ω_0) accounting for the effects of GVD and TOD. It readily emerges that as the initial pulse width decreases below 90 fs, the third-order dispersion effects start contributing and below 40 fs become too high that pulses with lesser width cannot be used for practical FSO communication systems.

A commonly used criterion for maintaining broadened pulse within the allocated bit slot is restricting $\sigma_1 = \Omega_B/4$, where 'Ω_B' is the allocated bit slot, which is related to the bit rate (B) through, $\Omega_B = 1/B$ [24]. The variation of the bit rate under the influence of GVD and TOD as a function of initial pulse width is shown in Fig. 2.

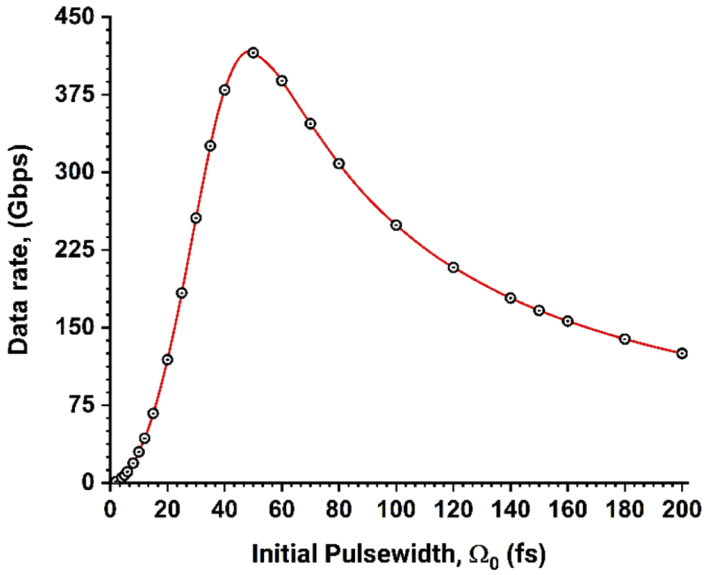

Fig. 2. Achievable data rate under pulse broadening conditions. A large drop in data rate can be observed for initial pulse widths less than 40 fs. This can be attributed to the large increase in the broadening due to TOD (Fig. 1, top panel for $\Omega_0 < 40$ fs).

It can be observed that, effect of TOD significantly influences pulse broadening (Fig. 1, top panel) and results into a large drop in the data rate below 40 fs. This sets a practical lower limit for the width of narrow optical pulses, that can be effectively used for FSO communication, with the advantage of higher data throughput with narrower pulses.

Optics EXPRESS

4.2. Enhanced pulse broadening due to aerosol radiative effects

In view of the above finding, we focus our attention on aerosol impacts on ultra-short optical pulses through turbulent atmosphere for pulse widths greater than 40 fs. Digital communication receivers integrate the received signals over a time-interval and decide upon the transmitted signal. Hence temporal broadening and subsequent overlapping of adjacent pulses would result in symbol estimation errors at the receiver electronics, commonly referred as inter-symbol interference (ISI). We have analyzed a 2 km long horizontal FSO link at an altitude of 1.75 km, operating at a wavelength of 1.55 μm. Without losing the generality, the pulse width was taken at the full width half maximum (FWHM) of on-axis intensity values to compute the broadening factor. We define C_n^2 as the refractive index structure parameter under unperturbed conditions, estimated through the measured meteorological profiles from radiosonde and C_n^{2*} as the same after accounting for the aerosol-perturbed conditions. To account for the large seasonal changes in aerosol single scattering albedo (SSA, which is an important parameter deciding the C_n^2 value through aerosol induced warming, is defined as the ratio of aerosol scattering to aerosol extinction), the perturbed states have been further extended for a sensitivity analysis by changing the aerosol SSA from 0.7 (when highly absorbing aerosol species such as soot or BC (emitted from the combustion of fossil fuels and biomass) constitutes to about 10% of the total aerosol load, a condition encountered in major urban centers) to 1.0 (purely scattering with no soot in the atmosphere).

Highly absorbing aerosols are characterized by lower values of SSA, whereas an SSA = 1 indicates purely scattering aerosols. Variation of C_n^2, C_n^{2*}, 'β_2' and 'β_3' with altitude have been estimated using radiosonde and satellite observations as detailed in the materials and methodology section. These vertical variations have been estimated at every 50-m height interval from the surface. Out of these estimates, we have chosen values for the specified parameters at 1.75 km to account for the extreme case scenario imparted by the aerosol perturbations. Aerosol perturbed C_n^2* were estimated from the aerosol radiative forcing calculations using SBDART for SSA values from 0.7 to 1 (at 0.5 increment). These values are listed in Table 1. To investigate the significance of optical properties of soot particles on the enhanced pulse broadening we have employed a hybrid approach using observed AOD from MODIS and OPAC model. The aerosol type and its default constituent components are maintained as such in the OPAC model; however, the BC number concentrations were changed to match the observed AOD. This iterative procedure repeated for each SSA value, to derive the mass fraction of BC through OPAC model. Mass fraction of BC varied from as high as 12.6% for SSA = 0.70, to zero for SSA = 1.

Table 1. Unperturbed refractive index structure parameter (C_n^2) and aerosol perturbed C_n^{2*} for various values of single scattering albedo (SSA).

SSA	C_n^2 ($\times 10^{-19}$ $m^{-2/3}$)	C_n^{2*} ($\times 10^{-14}$ $m^{-2/3}$)
0.70	2.4	6.01
0.75	2.4	5.28
0.80	2.4	4.57
0.85	2.4	3.22
0.90	2.4	1.79
0.95	2.4	1.53
1.00	2.4	0.972

Figure 3 illustrates the temporally broadened pulse against the time scale (t-z/c) for different values of SSA, estimated using Eq. (8) for an initial pulse width $\Omega_0 = 150$ fs using the corresponding values of C_n^2* from Table 1. The origin is at the peak of the Gaussian pulse. It can be observed that the temporal broadening of the pulse increases with decrease in SSA values (increasing

Optics EXPRESS

aerosol absorption), while the peak intensity decreases. These are attributed to the enhanced scintillation due to the local modulation of optical turbulence, indicated by the C_n^2* values (Table 1), by the absorbing aerosols which are characterized by smaller values of SSA.

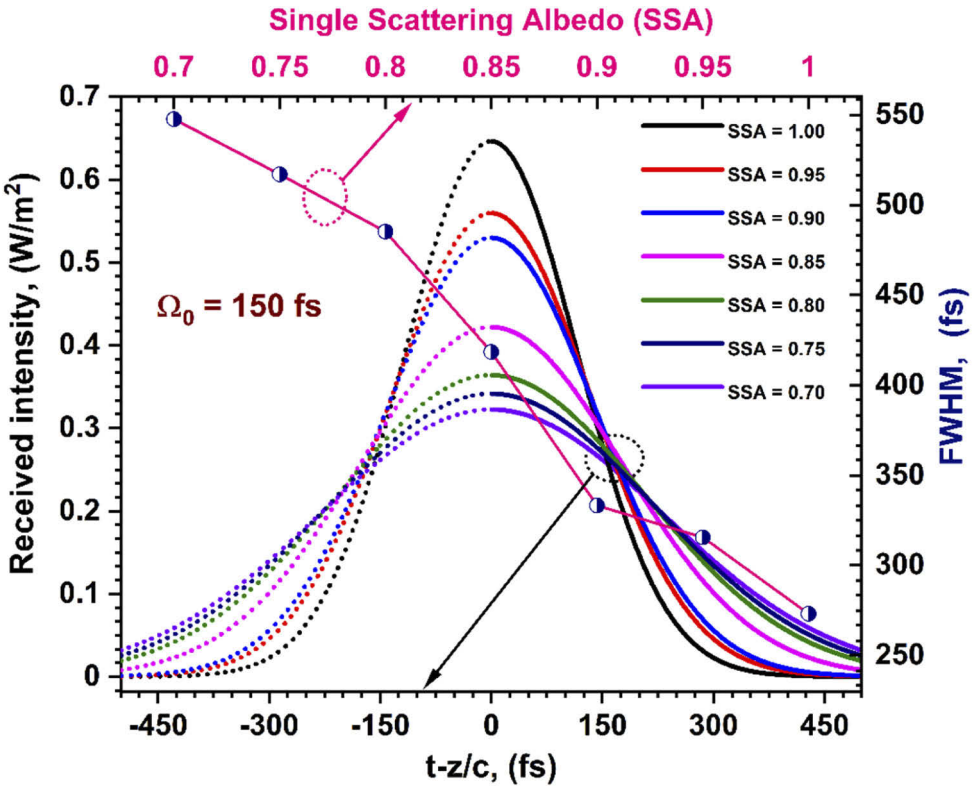

Fig. 3. Gaussian pulse at the receiver for various Single Scattering Albedo (SSA) values, showing enhanced broadening for smaller SSA. The origin is at peak of Gaussian pulse, with initial pulse width, $\Omega_0 = 150$ fs. The line curve with markers shows the Full Width Half Maximum (FWHM; right side Y axis) of the received pulse as a function of the SSA (top X axis). Arrows are used to point out the axes corresponding to different curves. Note that for SSA = 0.70, the pulse broadens by a factor ≈4 (i.e. FWHM/ Ω_0), while the broadening factor is < 2 when SSA=1.

The enhanced optical turbulence due to aerosol induced warming is manifested as refractive index fluctuations, causing different spectral components of the pulse to travel at different speeds, leading to pulse spreading. Besides enhancing the pulse broadening, the increased concentration of absorbing aerosols (lower SSA) also leads to reduction in signal due to the absorption. This reduction in intensity can set further constraint to the performance of the threshold detection digital receivers. Figure 3 further illustrates the variation of FWHM against SSA (right and top axes). Highest FWHM is observed for the least SSA due to the enhanced pulse broadening arising due to aerosol-induced atmospheric warming and decreases with increasing SSA. FWHM ranges up to 3–4 times initial pulse width (dependence of pulse broadening on initial pulse width is discussed further in Fig. 4) at lower SSA, while it is nearly twice the initial value above SSA = 0.90, where aerosol scattering effect is dominant. Thus, enhanced pulse broadening is predominantly due to higher absorbing aerosol fraction as indicated by the lower SSA.

Broadening factor under perturbed conditions ($BF_{perturbed}$) is defined as the ratio between pulse width of broadened pulse (Ω_2; due to enhanced optical turbulence by atmospheric aerosols

Optics EXPRESS

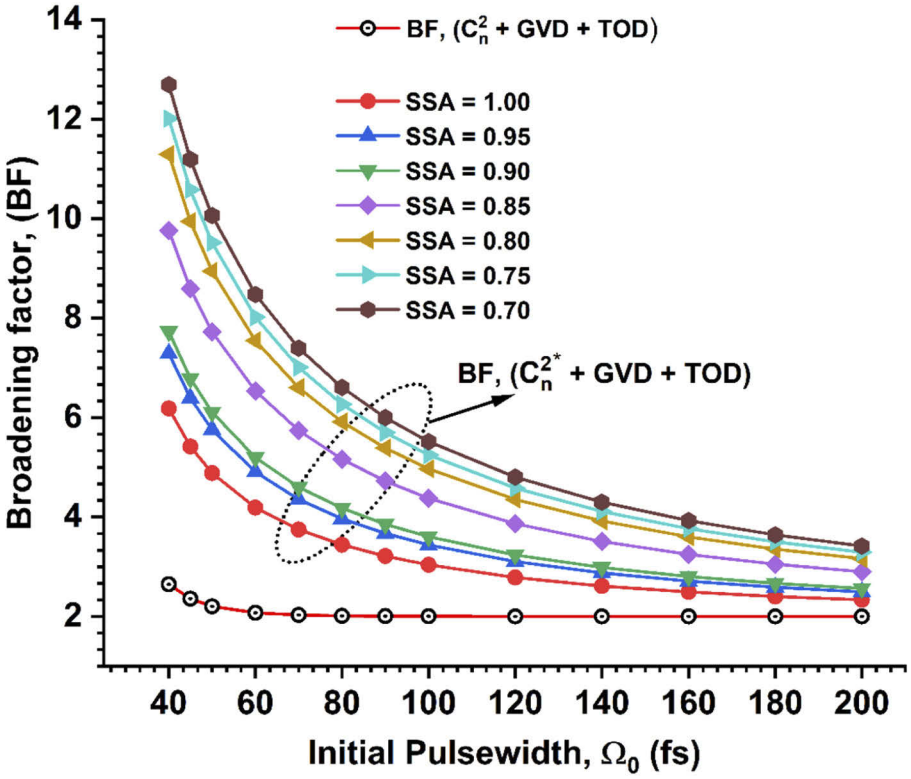

Fig. 4. Dependence of optical pulse broadening factor ($BF_{perturbed} = \Omega_2/\Omega_0$) on the input pulse width (Ω_0) and Single Scattering Albedo (SSA) of atmospheric aerosols. Significant difference in broadening factor can be observed between the conditions of C_n^2 and C_n^2* along with GVD and TOD.

characterized through C_n^2*) to its initial width (Ω_0). It is a useful parameter to decide the limit to which high-data rate optical systems can be operated without ISI. In Fig. 4, we have shown the variation of $BF_{perturbed}$ with initial pulse width and SSA of aerosols. In order to delineate the impact of atmospheric aerosols from other effects, pulse broadening due to GVD + TOD (estimated through Eq. (2), (3) and (7) using GPS radiosonde profiles) as discussed under Fig. 1, is also plotted in Fig. 4 (the bottom most curve). It clearly emerges that the impact of aerosol perturbed conditions (C_n^2*) on broadening factor is significantly higher than that due to unperturbed conditions (C_n^2) and can reach as high as 10 for very short pulses when SSA = 0.70.

With a view to delineating the effect of aerosols alone, we have plotted aerosol perturbed broadening factor ($BF_{perturbed}$) for two cases, viz. with and without the group velocity dispersion and third order dispersion effects, in Fig. 5. It is worthwhile to notice that the effect of GVD and TOD on pulse broadening is very less compared to the aerosol induced broadening (as long as the input pulse width is greater than 40 or 50 fs for reasons already explained in discussion of Fig. 1). It emerges that for any given SSA, narrower the pulse, higher is the $BF_{perturbed}$ while for a given pulse width, lower the SSA, higher is the $BF_{perturbed}$. The large difference in pulse broadening between narrow and wider pulses is attributed to the amplified scintillation imparted by absorbing aerosols and the spectral dependence of the velocity retardation of various frequency components. As SSA increases, perturbed optical turbulence decreases and consequently the broadening also decreases, with this effect being predominant on narrow pulses compared to wider pulses. The rate at which pulse broadens with SSA decreases with increase in the width of

Optics EXPRESS

the input pulses and becomes less significant for pulses larger than 150 fs, even though wider pulses reduce the information carrying capacity of optical channels. The increased slope along the SSA axis for pulse widths < 60 fs evidences the enhanced influence of absorbing aerosols on femtosecond pulses compared to wider pulses. Nonetheless, pulses >150 fs are relatively immune to aerosol-induced impairments.

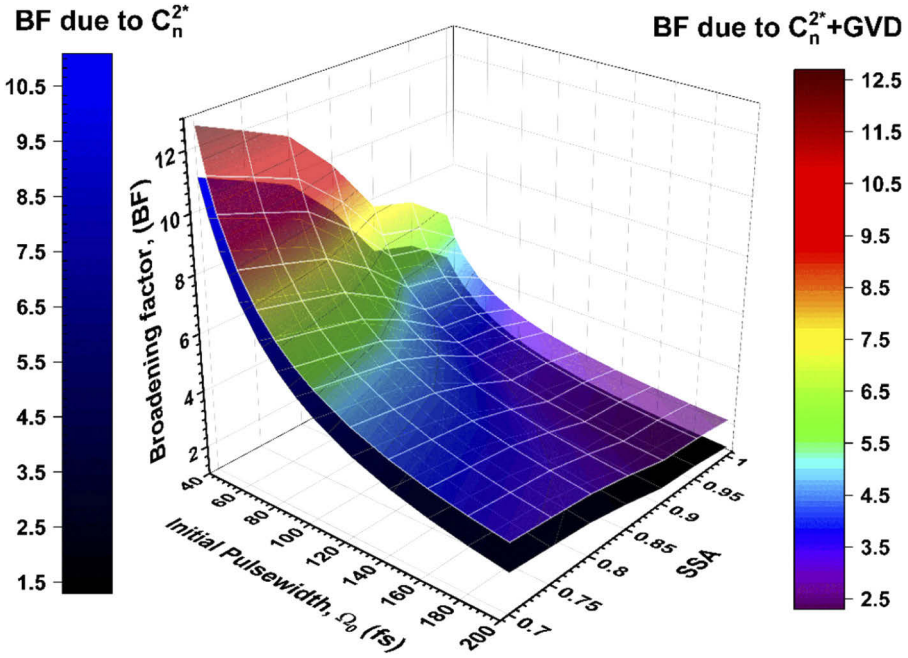

Fig. 5. Broadening factor due to perturbed aerosol conditions for various input pulse widths with and without GVD effects are shown.

We further examine the implication of the above in the energy content (we have used numerical integration technique for obtaining the area under the curve) of the received pulse by estimating the normalized energy ($E_N = E_2/E_0$) where, 'E_2' is the energy contained in the received pulse and 'E_0' the energy of the transmitted pulse. Normalized energy has been plotted in Fig. 6 for various input pulse width and SSA values. It is observed that the normalized pulse energy decreases with increasing input pulse width (pulses containing higher energy) and decreasing SSA. The nonlinear relationship between 'Ω_0' and normalized pulse energy (E_N) along with the defiance of wider pulses to aerosol-induced broadening causes the existence of gradient of normalized energy with respect to input pulse width, ($dE_N/d\Omega_0$). As the SSA increases from 0.70, the normalized energy increases, with narrow pulses taking higher fractional energy, which eventually becomes negligible above SSA = 0.90 and leads to $dE_N/d\Omega_0$ approaching zero. This is further substantiated by the perceptibly sharp increase in 'E_N' for a fixed initial pulse width with increasing SSA. Both $dE_N/d\Omega_0$ and slope along SSA axis ($dE_N/dSSA$) vanishes for all values of initial pulse widths when SSA exceeds 0.90.

This is attributed to the weakening of enhanced scintillation due to the less aerosol absorption with estimated $C_n^{2}*$ reaching 9.72×10^{-15} $m^{-2/3}$ at SSA = 1. The levelling of the curve above SSA = 0.90 further indicates that the influence of larger fraction of scattering aerosols is independent of the initial pulse width, unlike uneven absorption and pulse width dependent fractional distribution of normalized energy at lower SSA values. Residence of large concentration of absorbing aerosols over longer duration can thus adversely affect femtosecond pulsed FSO communication systems employing threshold detection receivers due to the uneven energy

Optics EXPRESS

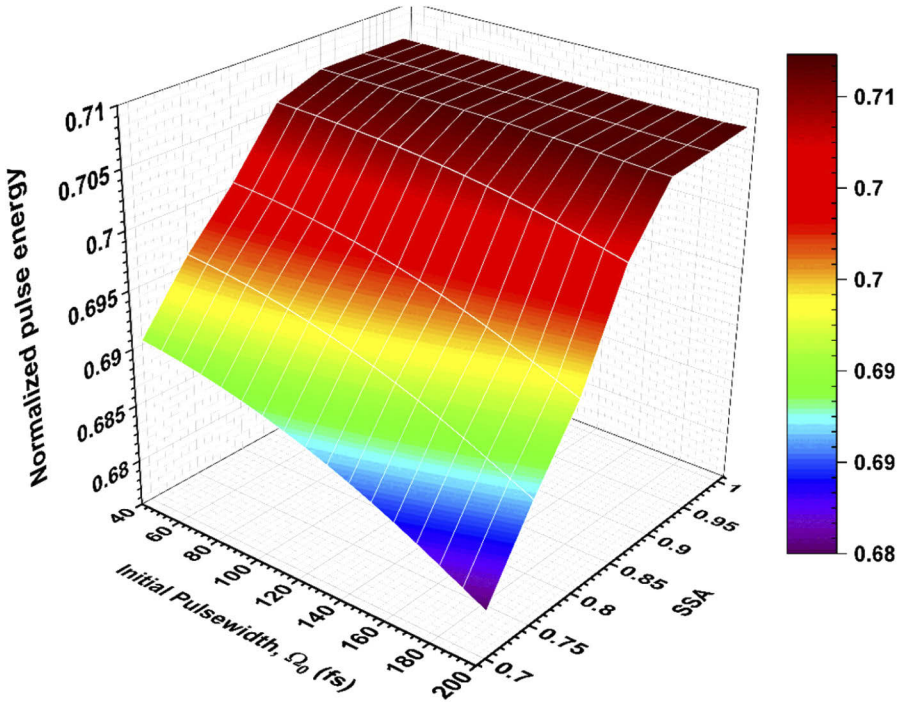

Fig. 6. Variation of normalized energy (E_N) of the received optical pulse with input pulse width (Ω_0) and Single Scattering Albedo (SSA) of atmospheric aerosols. As the SSA increases from 0.70, the normalized energy increases with narrow pulses taking higher fractional energy, which eventually becomes negligible above SSA = 0.90, $dE_N/d\Omega_0$ approaching zero.

redistribution produced by radiative heating in the lower troposphere. Impact of pulse broadening on the performance parameters of FSO systems is beyond the scope of the present study. Nonetheless, the present investigation unravels the role of lower atmospheric absorbing aerosols on the enhancement of temporal broadening of optical pulses.

5. Conclusions

The radiative effects of atmospheric aerosols on the propagation of optical pulses have been studied in detail in the context of FSO communication, using radiative transfer calculations incorporating in-situ and satellite observations of atmospheric thermodynamics and aerosols. Third order dispersion, along with group velocity dispersion, sets a practical lower limit of ~40 fs for the input pulse width, below which, there is a sharp deterioration in the data rate of FSO links. Our main findings are:

- Random variations in the atmospheric refractive index, resulting from aerosol-induced atmospheric heating, manifest as a dispersive channel and disproportionately affect the different spectral components of the transmitted pulse, leading to broadening and deterioration of the optical pulses.
- There is a large enhancement in the optical pulse broadening due to the perturbations in atmospheric refractive index structure parameter (C_n^2) by light-absorbing aerosols. Pulse broadening with broadening factor exceeding 10 is observed for pulses with width less than 60 fs, while pulse widths above 150 fs are not significantly affected by aerosols.

Optics EXPRESS

- For a given initial pulse width, there is an increase in the pulse broadening factor as the aerosol single scattering albedo (SSA) decreases. This effect is observed to increase with decreasing input pulse width. For SSA = 0.70, the pulse broadens by a factor ≈ 4 (i.e. FWHM/Ω_0), whereas the broadening factor is less than 2 for higher SSA values.
- Gradient of normalized pulse energy with initial pulse width is negative for lower aerosol SSA values and approaches zero for higher SSA values, causing the aerosol-induced optical pulse broadening to be independent of the initial pulse width in atmospheres with lesser absorbing aerosols.

Funding

DST-Centre of Excellence in Climate Change, Divecha Centre for Climate Change, Indian Institute of Science, Bengaluru.

Acknowledgments

We acknowledge the use of radiosonde data obtained from University of Wyoming through http://weather.uwyo.edu/upperair/sounding.html. The CALIPSO data were obtained from the NASA Langley Research Center Atmospheric Science Data Center (ASDC) through https://asdc.larc.nasa.gov/. MODIS level 2 albedo was acquired from https://modis.gsfc.nasa.gov/data/. We acknowledge the MODIS mission scientists and associated NASA personnel for the level 3 AOD data used in this work. One of the authors (SKS) thank J. C. Bose Fellowship from Department of Science and Technology, India. Anand acknowledges the Grantham fellowship awarded by Divecha Centre for Climate Change.

Disclosures

The authors declare no conflicts of interest.

References

1. S. Arnon, J. R. Barry, G. K. Karagiannidis, R. Schober, and M. Uysal Eds, *Advanced Optical Wireless Communication Systems* (Cambridge University, 2012).
2. M. Uysal, C. Capsoni, Z. Ghassemlooy, A. Boucouvalas, and E. Udvary, *Optical wireless communications: an emerging technology* (Springer, 2016).
3. L. C. Andrews, R. L. Phillips, and C. Y. Hopen, *Laser beam scintillation with applications*, (SPIE, 2001).
4. A. L. Steiner, D. Mermelstein, S. J. Cheng, T. E. Twine, and A. Oliphant, "Observed impact of atmospheric aerosols on the surface energy budget," Earth Interact. **17**(14), 1–22 (2013).
5. J. H. Seinfeld and S. N. Pandis, *Atmospheric Chemistry and Physics: From Air Pollution to Climate Change*, 2nd ed. (Wiley, 2006).
6. I. Dror and N. S. Kopeika, "Experimental comparison of turbulence modulation transfer function and aerosol modulation transfer function through the open atmosphere," J. Opt. Soc. Am. A **12**(5), 970–980 (1995).
7. D. Sadot and N. S. Kopeika, "Imaging through the atmosphere: practical instrumentation-based theory and verification of aerosol modulation transfer function," J. Opt. Soc. Am. A **10**(1), 172–179 (1993).
8. S. K. Satheesh, "Aerosol radiative forcing over land: effect of surface and cloud reflection," Ann. Geophys. **20**(12), 2105–2109 (2002).
9. S. K. Satheesh and V. Ramanathan, "Large differences in tropical aerosol forcing at the top of the atmosphere and Earth's surface," Nature **405**(6782), 60–63 (2000).
10. N. Anand, K. Sunilkumar, S. K. Satheesh, and K. K. Moorthy, "Distinctive roles of elevated absorbing aerosol layers on free-space optical communication systems," Appl. Opt. **57**(25), 7152–7158 (2018).
11. S. Butrimas, R. Driggers, G. Holst, N. S. Kopeika, and A. Zilberman, "Effects of aerosol modulation transfer function on target identification," Opt. Eng. **59**(07), 1 (2020).
12. C. H. Liu and K. C. Yeh, "Propagation of pulsed beam waves through turbulence, cloud, rain, or fog.," J. Opt. Soc. Am. A **67**(9), 1261–1266 (1977).
13. C. Y. Young, A. Ishimaru, and L. C. Andrews, "Two-frequency mutual coherence function of a Gaussian beam pulse in weak optical turbulence: an analytic solution," Appl. Opt. **35**(33), 6522–6526 (1996).
14. I. Sreenivasiah, A. Ishimaru, and S. T. Hong, "Two-frequency mutual coherence function and pulse propagation in a random medium: An analytical solution to plane wave case," Radio Sci. **11**(10), 775–778 (1976).

Optics EXPRESS

15. J. Libich, J. Perez, S. Zvanovec, Z. Ghassemlooy, R. Nebuloni, and C. Capsoni, "Combined effect of turbulence and aerosol on free-space optical links," Appl. Opt. **56**(2), 336–341 (2017).
16. W. G. Alheadary, K.-H. Park, N. Alfaraj, Y. Guo, E. Stegenburgs, T. K. Ng, B. S. Ooi, and M.-S. Alouini, "Free-space optical channel characterization and experimental validation in a coastal environment," Opt. Express. **26**(6), 6614–6628 (2018).
17. M. Arikawa and T. Ito, "Performance of mode diversity reception of a polarization-division-multiplexed signal for free-space optical communication under atmospheric turbulence," Opt. Express **26**(22), 28263–28276 (2018).
18. N. Anand, K. Sunilkumar, S. K. Satheesh, and K. K. Moorthy, "Entanglement of near-surface optical turbulence to atmospheric boundary layer dynamics and particulate concentration: implications for optical wireless communication systems," Appl. Opt. **59**(5), 1471–1483 (2020).
19. K. Sunilkumar, N. Anand, S. K. Satheesh, K. K. Moorthy, and G. Ilavazhagan, "Performance of free-space optical communication systems: effect of aerosol-induced lower atmospheric warming," Opt. Express **27**(8), 11303–11311 (2019).
20. S. Bendersky, N. Kopeika, and N. Blaunstein, "Effects of attenuation of 1.064-μm optical waves by humid aerosols and fog over horizontal atmospheric communication links," Opt. Eng. **43**(3), 539–552 (2004).
21. S. Arnon and N. S. Kopeika, "Effect of particulates on performance of optical communication in space and an adaptive method to minimize such effects," Appl. Opt. **33**(21), 4930–4937 (1994).
22. K. Sunilkumar, N. Anand, S. K. Satheesh, and G. Ilavazhagan, "Radiative effects of atmospheric aerosols on optical pulse propagation: implications to high data rate Free Space Optical (FSO) communication systems," *Proc. SPIE 11133, Laser Communication and Propagation through the Atmosphere and Oceans VIII*, 1113310 (6 September 2019).
23. N. Anand, S. K. Satheesh, and K. K. Moorthy, "Dependence of atmospheric refractive index structure parameter (C_n^2) on the residence time and vertical distribution of aerosols," Opt. Lett. **42**(14), 2714–2717 (2017).
24. G. P. Agarwal, *Fiber-optic communication systems*, 3rd ed. (John Wiley & Sons, 2001).
25. N. Stassinakis, H. E. Nistazakis, K. P. Peppas, and G. S. Tombras, "Improving the availability of terrestrial FSO links over log normal atmospheric turbulence channels using dispersive chirped Gaussian pulses," Opt. Laser Technol. **54**, 329–334 (2013).
26. K. N. Liou, *An introduction to atmospheric radiation*, Vol. 84, (Elsevier, 2002).
27. K. Stamnes, S. C. Tsay, W. Wiscombe, and K. Jayaweera, "Numerically stable algorithm for discrete-ordinate-method radiative transfer in multiple scattering and emitting layered media," Appl. Opt. **27**(12), 2502–2509 (1988).
28. D. Nath, M. Venkat Ratnam, A. K. Patra, B. V. Krishna Murthy, and S. V. Bhaskar Rao, "Turbulence characteristics over tropical station Gadanki (13.5 N, 79.2 E) estimated using high-resolution GPS radiosonde data," J. Geophys. Res. **115**(D7), D07102 (2010).
29. S. S. Babu, K. K. Moorthy, and S. K. Satheesh, "Vertical and horizontal gradients in aerosol black carbon and its mass fraction to composite aerosols over the east coast of Peninsular India from Aircraft measurements," Advances in Meteorology **2010**, 1–7 (2010).
30. N. Anand, K. Sunilkumar, S. K. Satheesh, and K. K. Moorthy, "Dual role of absorbing aerosols in atmospheric refractive index fluctuations: a closure study from balloon-based and multi-satellite observations," *Proc. SPIE 11133, Laser Communication and Propagation through the Atmosphere and Oceans VIII*, 1113311 (6 September 2019).
31. P. Ricchiazzi, S. Yang, C. Gautier, and D. Sowle, "SBDART, a research and teaching tool for plane-parallel radiative transfer in the Earth's atmosphere," Bull. Am. Meteorol. Soc. **79**(10), 2101–2114 (1998).
32. M. Hess, P. Koepke, and I. Schult, "Optical properties of aerosols and clouds: the software package OPAC," Bull. Am. Meteorol. Soc. **79**(5), 831–844 (1998).
33. S. E. Schwartz, "The whitehouse effect: Shortwave radiative forcing of climate by anthropogenic aerosols: An overview," J. Aerosol Sci. **27**(3), 359–382 (1996).
34. H. Lu, W. Zhao, and X. Xie, "Analysis of temporal broadening of optical pulses by atmospheric dispersion in laser communication system," Opt. Commun. **285**(13-14), 3169–3173 (2012).
35. C. Y. Young, L. C. Andrews, and A. Ishimaru, "Time-of-arrival fluctuations of a space time Gaussian pulse in weak optical turbulence: an analytic solution," Appl. Opt. **37**(33), 7655–7660 (1998).